AD-A280 958

DOCUMENTATION PAGE

1a. REPORT SECURITY CLASSIFICATION: Unclassified	1b. RESTRICTIVE MARKINGS
2a. SECURITY CLASSIFICATION AUTHO	3. DISTRIBUTION/AVAILABILITY OF REPORT: This document has been approved for public release and sale; it's distribution is unlimited
2b. DECLASSIFICATION/DOWNGRADING SCHEDULE	
4. PERFORMING ORGANIZATION REPORT NUMBER(S): Technical Report #1	5. MONITORING ORGANIZATION REPORT NUMBER(S): 4133046
6a. NAME OF PERFORMING ORGANIZATION: University of Minnesota; 6b. OFFICE SYMBOL (If applicable): ONR	7a. NAME OF MONITORING ORGANIZATION: Office of Naval Research
6c. ADDRESS (City, State, and ZIP Code): Dept. of Chemical Eng. & Materials Science, University of Minnesota, Minneapolis, MN 55455	7b. ADDRESS (City, State, and ZIP Code): 800 Quincy Street North, Arlington, VA 22217-5000
8a. NAME OF FUNDING/SPONSORING ORGANIZATION: Office of Naval Research; 8b. OFFICE SYMBOL (If applicable): ONR	9. PROCUREMENT INSTRUMENT IDENTIFICATION NUMBER: Grant NO0014-93-1-0563
8c. ADDRESS (City, State, and ZIP Code): 800 North Quincy Street, Arlington, VA 22217-5000	10. SOURCE OF FUNDING NUMBERS: PROGRAM ELEMENT NO. / PROJECT NO. / TASK NO. / WORK UNIT ACCESSION NO

11. TITLE (Include Security Classification)
Atomic Force Microscopy of the Electrochemical Nucleation and Growth of Molecular Crystals

12. PERSONAL AUTHOR(S)
A. C. Hillier and M. D. Ward

13a. TYPE OF REPORT	13b. TIME COVERED	14. DATE OF REPORT (Year, Month, Day)	15. PAGE COUNT
Technical	FROM 5/1/93 TO 6/30/94	6/23/94	19

16. SUPPLEMENTARY NOTATION

17. COSATI CODES		
FIELD	GROUP	SUB-GROUP

18. SUBJECT TERMS (Continue on reverse if necessary and identify by block number)
Organic Conductors/Atomic Force Microscopy/Nucleation/ Fractals

19. ABSTRACT (Continue on reverse if necessary and identify by block number)

In situ atomic force microscopy reveals the morphology, surface topography, and growth and dissolution characteristics of microscopic single crystals of the low dimensional organic conductor (tetrathiafulvalene)$Br_{0.76}$, which are grown by electrocrystallization on a highly oriented pyrolytic graphite electrode in an atomic force microscope liquid cell. The growth modes, and the distribution and orientation of topographic features (i.e., terraces, ledges, and kinks) on specific crystal faces, as assigned by "atomic force microscopy goniometry," can be correlated with the strength and direction of anisotropic solid state intermolecular bonding. The influence of substrate structure was evident during growth on the (011) face of (tetrathiafulvalene)$Br_{0.76}$ crystals, which involves the formation of oriented self-similar triangular islands ranging from 200 Å to 5000 Å along a side. These nuclei eventually transform into rectangular rafts at larger length scales, where bulk intermolecular bonding interactions and surface energies dominate over nuclei-substrate interactions.

20. DISTRIBUTION/AVAILABILITY OF ABSTRACT: ☒ UNCLASSIFIED/UNLIMITED ☐ SAME AS RPT ☐ DTIC USERS	21. ABSTRACT SECURITY CLASSIFICATION: Unclassified
22a. NAME OF RESPONSIBLE INDIVIDUAL: Robert Nowak	22b. TELEPHONE (Include Area Code): (612) 703-696-4409; 22c. OFFICE SYMBOL: ONR Code 1113

DD FORM 1473, 84 MAR — 83 APR edition may be used until exhausted. All other editions are obsolete

SECURITY CLASSIFICATION OF THIS PAGE: Unclassified

C -FICE OF NAVAL RESEARCH

GRANT # N00014-93-1-0563

R&T Code 4133046

Technical Report # 1

"Atomic Force Microscopy of the Electrochemical Nucleation and Growth of Molecular Crystals"

by

A. C. Hillier and M. D. Ward

Prepared for Publication

in

Science

Department of Chemical Engineering and Materials Science
University of Minnesota
Amundson Hall
421 Washington Ave. SE
Minneapolis, MN 55455

June 20, 1994

Atomic Force Microscopy of the Electrochemical Nucleation and Growth of Molecular Crystals

Andrew C. Hillier and Michael D. Ward*
Department of Chemical Engineering and Materials Science
University of Minnesota, Amundson Hall
421 Washington Ave. SE, Minneapolis, MN 55455

In situ atomic force microscopy reveals the morphology, surface topography, and growth and dissolution characteristics of microscopic single crystals of the low dimensional organic conductor (tetrathiafulvalene)$Br_{0.76}$, which are grown by electrocrystallization on a highly oriented pyrolytic graphite electrode in an atomic force microscope liquid cell. The growth modes, and the distribution and orientation of topographic features (i.e., terraces, ledges, and kinks) on specific crystal faces, as assigned by "atomic force microscope goniometry," can be correlated with the strength and direction of anisotropic solid state intermolecular bonding. The influence of substrate structure was evident during growth on the (011) face of (tetrathiafulvalene)$Br_{0.76}$ crystals, which involves the formation of oriented self-similar triangular islands ranging from 200 Å to 5000 Å along a side. These nuclei eventually transform into rectangular rafts at larger length scales, where bulk intermolecular bonding interactions and surface energies dominate over nuclei-substrate interactions.

*Author to whom correspondence should be addressed
Version 2.2 : January 12, 1994

Molecular crystals containing organic components exhibit a variety of electronic properties, including electrical conductivity, superconductivity, non-linear optical behavior, and ferromagnetism, (*1*) and also comprise the majority of pharmaceutical reagents. (*2*) Much of the interest in these materials stems from the ability to employ molecular-level "crystal engineering" strategies (*3*) to control solid state intermolecular interactions in order to rationally manipulate crystal packing and, consequently, influence bulk physical and electronic properties. While these strategies have been employed in the design and synthesis of many organic crystals, the self-assembly, nucleation, and crystallization processes that are responsible for their formation are not well understood, particularly at the molecular and nanoscale level. This understanding is crucial if important crystal characteristics such as polymorphism, morphology, inclusion formation, and defect density are to be controlled.

Recent developments in atomic force microscopy (AFM), (*4*) however, now provide for in situ visualization of the early stages of growth of organic crystals in liquids, as evidenced by recent reports for these and other materials. (*5,6,7*) This capability provides for dynamic observation of nucleation events, and the determination, at small length scales, of the distribution of topographic features (i.e. terraces, ledges and kinks) that play an important role in crystal growth. (*8*) We herein describe in situ AFM observations of the electrochemical nucleation and growth of the crystalline quasi one-dimensional organic conductor (TTF)$Br_{0.76}$ (TTF = tetrathiafulvalene), (*9*) wherein the rate of crystal growth was regulated by the electrochemical potential applied during the electrocrystallization process. (*10*) Electrocrystallization is a convenient method for AFM visualization of crystal growth modes because the supersaturation at the crystal surface can be controlled by the electrochemical potential, analogous to the effect of changing solute concentration during the growth of non-conducting crystals. (TTF)$Br_{0.76}$ was the system of choice for this study because it is representative of low dimensional organic conductors, and previous studies indicated that growth occurred readily on existing nuclei during electrocrystallization. (11) In the present work, distinct crystal faces of microscopic (TTF)$Br_{0.76}$ crystals have been observed and

identified by AFM goniometry, with the assignments confirmed by comparison of high resolution AFM images with the single crystal x-ray structure. We have been able to visualize the nucleation and growth modes on different crystal faces under controlled conditions, and have observed highly unusual, oriented triangular nuclei growing on the (011) face of $(TTF)Br_{0.76}$. These studies illustrate the roles of intermolecular bonding, surface energies, and substrate-nuclei interactions on crystal topography, nuclei morphology, and growth at small length scales.

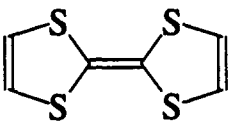

TTF

Electrochemical nucleation and growth of well-defined needle crystals of the conductive, nonstoichiometric salt $(TTF)Br_{0.76}$ on a freshly cleaved, highly oriented pyrolytic graphite (HOPG) electrode was accomplished readily in an AFM liquid cell (eq. 1). (*12*) Crystallization was induced by the brief application (1-5 seconds) of an anodic potential step in the range $0.40 \leq E_{applied} \leq 0.70$ V (vs. SCE). (*13*) Under these conditions, AFM revealed nucleation of $(TTF)Br_{0.76}$ crystals on the HOPG electrode, with nucleation densities approaching 10^3 mm^{-2}. These needle crystals exhibited widths ranging from 0.2 - 4 μm, lengths of 10 -15 μm and heights of 0.1 - 0.75 μm. The needle axis of the crystals was always parallel to the HOPG substrate, but no azimuthal orientation was observed. (14) Subsequent growth or dissolution of these crystals could be precisely controlled by selection of the applied electrochemical potential.

$$TTF + 0.76\ Br^- \rightarrow (TTF)Br_{0.76} + 0.76\ e^- \qquad (1)$$

The microscopic $(TTF)Br_{0.76}$ crystals exhibited several distinct faces, each with a unique morphology and topography (Fig. 1). The most prominent face was parallel to the substrate and extended along the needle axis of the crystal. This plane was identified as (010) by comparison of

high resolution AFM data to the molecular packing of this plane. (*15*) The periodicity of contrast was 15.01 Å and 3.25 Å along [100] and [001], respectively, in good agreement with the x-ray structure values of 15.617 Å and 3.572 Å. Molecular resolution on the other faces proved difficult due to the highly stepped nature of these faces. (*16*) However, the remaining faces could be assigned by "AFM goniometry" in which the dihedral angles between the faces were measured from AFM height data. (*17*) A self-consistent set for the observed planes includes (010), ($\bar{3}$10), and (210), which are parallel to [001], and (011) appearing on the crystal apex. (*18,19*) The ($\bar{3}$11) and (211) planes were also occasionally observed at the tip of the crystal. (*20*)

[Figure 1]

The closely packed (010) face exhibits [001] ledges with step heights of 6.3 - 7.2 Å, in good agreement with the TTF layer spacing normal to the (010) plane (Fig. 2). The [001] ledges are enforced by strong intermolecular bonding energies ($\phi_{[001]}$) (*21*) along the [001] stacking axis associated with π-π charge transfer interactions between TTF molecules. The average width of the (010) terraces exceeds 3000 Å, reflecting a large $\phi_{[100]}$ value that can be attributed to electrostatic interactions between stacks of TTF^+ cations and the Br^- counterions along [100]. The presence of two strong in-plane bonding interactions in (010) provides for a low surface energy, $\gamma_{(010)}$, and the large area of this face in macroscopic crystals. (*8,22*) In addition, real-time imaging of growth on the (010) face indicates a two-dimensional nucleation and growth mode, consistent with two strong bonding vectors in this plane.

[Figure 2]

In contrast to (010), AFM data indicates that the ($\bar{3}$10) face is described by a high density of [001] ledges with step heights of 15 or 21 Å, equivalent to two or three TTF layers, respectively.

The average width of these ledges is < 25 Å. The ($\bar{3}$10) face is therefore best described as a high energy, highly stepped, vicinal face containing (010) terraces and (100) steps of molecular dimensions. The mode of crystal growth on ($\bar{3}$10) differs considerably from that observed on (010), occurring by the relatively rapid advancement of kinks along the [001] ledges, consistent with favorable intermolecular bonding ($\phi_{[001]}$) along this direction. These kinks are evident as features parallel to [$\bar{1}$30]. This process leads to accumulation on the [001] ledges and consequently, their advancement along [100]. The ($\bar{3}$10) face grows out of existence at larger length scales by bunching of the ledges, thereby generating the large (010) terraces. These results indicate that the surface topography and growth modes observed on (TTF)$Br_{0.76}$ crystals can be rationalized on the basis of solid-state intermolecular bonding interactions that exist within the plane of each distinct crystal face. The slow two-dimensional growth observed on (010) and the ledge bunching on ($\bar{3}$10) conspire to give the (010) face a large morphological importance in the macroscopic crystal.

Crystal planes exposed on the tip of a (TTF)$Br_{0.76}$ crystal, however, do not contain the [001] stacking axis. As a result, these faces tend to be microscopically rough and the corresponding growth mechanism does not appear to involve clearly defined ledges. The (011) face, which is the predominant face exposed upon the tip of a (TTF)$Br_{0.76}$ crystal, exhibits a pyramidal habit, intersecting the ($\bar{3}$10) and (210) planes along the [13$\bar{3}$] and [$\bar{1}$2$\bar{2}$] zones (Fig. 1a). Notably, nucleation on (011) occurs with the formation of *oriented triangular nuclei* (Fig. 3). One edge of the triangles is oriented at angle of 23° with respect to [13$\bar{3}$]. Initially, these triangular features exhibit dimensions of 200 Å on a side (area ≈ 90 nm^2) and 50 Å in height, evolving over time to 5000 Å on a side and 300 Å in height. These nuclei exhibit remarkable self-similarity over this entire size range, maintaining their orientation and aspect ratio. Indeed, the larger triangles are frequently observed as aggregates of smaller ones of the same orientation; consequently, they exhibit a "fractal" structure, resembling disordered Sierpinski gaskets (Fig. 3b and c). (*23*) The

size distribution of the smaller triangles comprising the gaskets appears to be fairly uniform, in contrast to true ordered Sierpinski gaskets, which are constructed from a generator that results in an ensemble of self-similar triangles of different sizes. Under the conditions where these gaskets are observed, the aggregation of the smaller triangles may occur by either diffusion along the (011) surface until attachment to other nuclei, or more likely, by a nucleation-redissolution mechanism in which small triangular nuclei persist upon aggregation with others.

[Figure 3]

The (011) plane of $(TTF)Br_{0.76}$ is best described as a highly stepped, vicinal plane consisting of [100] oriented ledges comprising mono-molecular (001) step planes and (010) terraces (Fig. 4). Furthermore, the [100] ledges contain molecular kink sites that are a consequence of the alternating orientation of the TTF molecules along this direction. Notably, a triangular array of these kinks can be constructed (denoted A in Fig. 4) whose orientation is identical to that of the triangular nuclei on the (011) face. This strongly supports a mechanism in which the observed nucleation behavior involves preferential attachment of incoming solute molecules to these kink sites and fast aggregation between these sites along directions corresponding to the edges of the triangles. While it may seem surprising that an opposite orientation is not observed (denoted B in Fig. 4), the two orientations are crystallographically unique under the symmetry of the monoclinic space group. Apparently, the chemical inequivalence resulting from the crystallographic inequivalence is sufficient to provide discrimination between the two orientations.

[Figure 4]

The triangular features observed during early stages of growth eventually evolve into oriented rectangular rafts whose long axis is parallel to [100] (Fig. 3d and e). This suggest that the

formation of the triangular nuclei results from a kinetic preference for the quasi-three fold (011) kink sites, whereas at larger length scales factors such as bulk thermodynamic bonding and surface energy supersede these interactions. The dominant intermolecular bonding within the (011) face is the electrostatic interaction along [100], which enforces the [100] ledge structure. The observed morphology after this transformation is indicative of the strong electrostatic $\phi_{[100]}$ bonding in the bulk and the more favorable surface energy of planes associated with the growth along [100], which overrides the substrate-nuclei interactions as the nuclei become larger. Indeed, the crystal faces exposed on the sides of the triangular nuclei will have a substantial surface energy due to their roughness.

We have demonstrated that electrochemical nucleation and growth of conducting molecular crystals can be visualized in situ at the nanoscale with the atomic force microscope, and that AFM goniometry can be performed to index micron-sized crystals, enabling comparison of crystal morphologies over several length scales. Our results clearly indicate that the surface topography and crystal growth modes depend upon the crystal face, generally reflecting the strength of intermolecular solid state bonding within the crystallographic planes defining those faces. However, it is evident that the molecular-level topography, such as that of the (011) face of $(TTF)Br_{0.76}$, can strongly influence morphology in the early stages of nucleation where substrate-nuclei interactions can predominate over bonding enthalpies in the bulk and surface energies that are important at large length scales. Further examination of nucleation and growth at the nanoscale will likely lead to other unanticipated length scale dependent behaviors, while providing an opportunity to unravel the fundamental principles that control crystal growth at the molecular level.

References

1. (a) J.S. Miller, A.J. Epstein, W.M. Reiff, *Science* **240**, 40 (1988). (b) J.S. Miller, *Extended Linear Chain Compounds* (Plenum, New York, 1982), vol. 1-3. (c) A.F. Garito and A.J. Heeger, *Acc. Chem. Res.* **7**, 232 (1974). (d) J.B. Torrance, *Acc. Chem. Res.* **12**, 79 (1979). (e) J. Zyss and G. Tsoucaris, *Structure and Properties of Molecular Crystals*, M. Pierrot, Ed. (Elsevier, Amsterdam, 1990), pp. 297-350.

2. S.R. Byrn, *Solid State Chemistry of Drugs*, (Academic Press, New York, 1982).

3. (a) G. M. J. Schmidt, *Pure Appl. Chem.* **27**, 647, (1971). (b) G. Desiraju, *Crystal Engineering - The Design of Organic Solids* (Elsevier, New York, 1989). (c) J.M. Lehn, *Angew. Chem., Int. Ed. Eng.* **27**, 89 (1988). (d) P.J. Fagan, M.D. Ward, J.C. Calabrese, *J. Am. Chem. Soc.* **111**, 1698 (1989).

4. (a) G. Binnig, C.F. Quate, Ch. Gerber, *Phys. Rev. Lett.* **12**, 930 (1986). (b) G. Binnig, Ch. Gerber, E. Stoll, T.R. Albrecht, C.F. Quate, *Europhys. Lett.* **3**, 1281 (1987).

5. (a) A.J. Gratz, S. Manne, P.K. Hansma, *Science* **251**, 1343 (1991). (b) P.E. Hillner, S. Manne, A.J. Gratz, P.K. Hansma, *Ultramicroscopy* **42-44**, 1387 (1992). (c) P.E. Hillner, A.J. Gratz, S. Manne, P.K. Hansma, *Geology* **20**, 359 (1992). (d) S.D. Durbin and W.E. Carlson, *J. Cryst. Growth* **122**, 71 (1992). (e) S.J. Manne, J.P. Cleveland, G.D. Stucky, P.K. Hansma, *J. Cryst. Growth* **130**, 333 (1993).

6. (a) B. Drake, et al., *Science* **243**, 1586 (1989). (b) O. Marti, B. Drake, P.K. Hansma, *Appl. Phys. Lett.* **51**, 17 (1987). (c) S. Manne, H.J. Butt, A.C. Gould, P.K. Hansma, *Appl. Phys. Lett.* **56**, 1758 (1990). (d) S. Manne, J. Massie, V.B. Elings, P.K. Hansma, A.A. Gewirth, *J. Vac. Sci. Technol.* **B9**, 950 (1991). (e) C. Chen and A.A. Gewirth, *Ultramicroscopy* **42-44**, 437 (1992).

7. (a) F. Ohnesorge and G. Binnig, *Science* **260**, 1451 (1993). (b) A.L. Weisenhorn, P.K. Hansma, T.R. Albrecht, C.F. Quate, *Appl. Phys. Lett.* **54**(26), 2651 (1989). (c) J. L. Hutter and J. Bechhoefer, *J. Appl. Phys.* **73**(9), 4123 (1993).

8. P. W. Carter, A. C. Hillier, M. D. Ward, *J. Am. Chem. Soc.* in press.

9. (a) F.B. Kaufman, E.M. Engler, D.C. Green, J.Q. Chambers, *J. Am. Chem. Soc.* **98**, 1596 (1976). (b) P. Kathirgamanathan and D.R. Rosseinsky, *J.C.S. Chem. Comm.*, 356 (1980). (c) P.A.C. Gane, P. Kathirgamanathan, D.R. Rosseinsky, *J.C.S. Chem. Comm.*, 378 (1981). (d) M. Lamache and K.E. Kacemi, *Mol. Cryst. Liq. Cryst.* **120**, 255 (1985). (e) J.B. Torrance and B.D. Silverman, *Phys. Rev. B*, **15**, 788 (1977). The true composition of the conductive $(TTF)Br_x$ salt ranges from $0.72 < x < 0.80$. The composition defines the extent of oxidation of the TTF chains, with the anions serving to neutralize charge. The value of $x = 0.76$ was chosen as it represents the average composition of the mixed valent $(TTF)Br_x$ salt.

10. M.D. Ward, *Electroanalytical Chemistry* (Marcel Dekker, Inc., New York, 1990), and references therein.

11. M.D. Ward, *J. Electroanal. Chem.*, **135**, 2747 (1988).

12. Atomic force microscopy experiments were performed with a Digital Instruments Nanoscope III scanning probe microscope equipped with a scan head having a maximal scan range of 125 x 125 x 5 μm^3 and with Nanoprobe™ cantilevers (Si_3N_4 with integral tips having spring constants of 0.06 Nm^{-1}). Images were obtained simultaneously in both constant force and error modes with filters off, an integral gain of 3.0, a proportional gain of 7.0, and a look-ahead gain of 0.0. The error mode, equivalent to a height image that has been high pass filtered, provides enhanced contrast. The AFM electrochemical cell (Digital Instruments) consisted of a freshly cleaved highly oriented pyrolytic graphite (HOPG) working electrode, a platinum counter electrode and a silver quasi-reference electrode. The HOPG electrode exhibited well defined atomic structure and nanometer scale flatness over length scales of tens

of microns. The electrolyte solution consisted of 5 mM TTF (Aldrich) in a 0.1 M solution of n-$Bu_4N^+Br^-$ (Aldrich) in ethanol.

13. Redox potentials for TTF: $E^o_{0/+}$ = 300 mV; $E^o_{+/2+}$ = 660 mV vs SCE.

14. This is the common crystal growth orientation in the AFM electrochemical fluid cell due to the restricted cell geometry. When an electrochemical cell that allows isotropic transport is employed, growth of $(TTF)Br_{0.76}$ crystals generally occurs with a random colatitudinal orientation. The AFM fluid cell geometry is thin and the counter electrode placement results in enhanced migration parallel to the HOPG surface, which favors the observed lateral growth.

15. The single crystal x-ray structure of $(TTF)Br_{0.76}$ reveals separate TTF and Br sublattices, which both pack in the monoclinic C2/m space group. See: (a) B.A. Scott, S.J. La Placa, J.B. Torrance, B.D. Silverman, B. Welber, *J. Am. Chem. Soc.* **99**, 6631 (1977). (b) S.J. La Placa, P.W.R. Cornfield, R. Thomas, B.A. Scott, *Solid State Comm.* **17**, 635 (1975). (c) G. Theodorou, *Phys. Rev. B*, **19**, 1132 (1979). Lattice parameters for the C2/m TTF sublattice: a_{TTF} = 15.617 Å, b_{TTF} = 15.627 Å, c_{TTF} = 3.572 Å, and β_{TTF} = 91.23° ; for the C2/m Br sublattice: a_{Br} = 17.368 Å, b_{Br} = 15.623 Å, c_{Br} = 4.538 Å, and β_{Br} = 116.01°. The sublattices have identical [010] lattice parameters, but the cell length of the Br sublattice along [001] is longer than that of the TTF sublattice, and the [100] directions of the sublattices subtend an angle of 24.8°. Therefore, it is more convenient from the standpoint of interpreting AFM data to describe the structure of $(TTF)Br_{0.76}$ by a supercell based on the isomorphic salt $(TTF)I_x$ (x = 5/7), whose structure has been solved according to a common monoclinic $P2_1/a$ space group, which incorporates both the anion and cation sublattices into a single unit cell with a = 48.165 Å (46.851Å), b = 16.052 Å (15.627 Å), c = 24.943 Å (25.004 Å), and β = 91.13° (91.23°). See: J.J. Daly and F. Sanz, *Acta Cryst.* **B31**, 620 (1975). (b) C.K. Johnson and C.R. Watson, *J. Chem. Phys.* **64**, 2271 (1976).

16. Typical AFM scanning tips have a radius of curvature ranging from 200 to 2000 Å, as determined by SEM. The interaction region between tip and sample has an area of magnitude. In order to obtain meaningful information regarding molecular level registry, then, the tip must be able to interact with a surface that is molecularly smooth over a size that is considerably larger than the interaction area of tip and sample. Therefore, the AFM cannot obtain lateral molecular level resolution on a surface containing a high density of ledges. The height of these steps, however, can be accurately determined to within a fraction of an angstrom.
17. As a note of caution, the resolution that may be obtained when measuring a dihedral angle with the AFM depends upon the aspect ratio of the cantilever tip. The maximum measurable angle between a terrace and a step plane is 55° using typical Si_3N_4 AFM tips with a 1:1 aspect ratio, whereas the maximum measurable angle using Si cantilevers with a 3:1 aspect ratio is 75°. For most of the experiments described in this report, Si_3N_4 cantilevers were employed. However, when the observed angle approached 55°, a Si cantilever was employed to verify the results.
18. Dihedral angles measured by AFM compared to those determined from the x-ray crystal structure (in parentheses) of the $(TTF)I_{5/7}$ supercell: (010) ∩ (210) = 36° (34°); (010) ∩ ($\bar{3}$10) = 43° (45°); (010) ∩ (011) = 33° (33°); (210) ∩ (011) = 50° (45°); ($\bar{3}$10) ∩ (011) = 50° (54°). These dihedral angles, as measured with AFM, were independent of the azimuthal orientation of the $(TTF)Br_{0.76}$ crystals with respect to the AFM tip. This morphology was also corroborated by scanning electron microscopy of crystals of similar size. These observations rule out artifacts due to tip geometry in the measurements of the dihedral angles.
19. The structure of $(TTF)Br_{0.76}$ is monoclinic and, thus, exhibits crystallographically (and chemically) distinct (100) and (010) faces. However, the difference between these planes results from only a 1.23° (β = 91.23°) offset of the TTF molecules in the (010) plane, as compared to (100). This difference is too slight to be differentiated using the interfacial angles or the high resolution molecular level registry as determined using the AFM. Thus, an

alternative assignment of the exposed faces of Figure 1 would be (100), (310), and (4$\bar{1}$0) along the [001] zone, and (103) at the crystal tip. Use of these alternative assignments would not alter the interpretation of the nucleation and growth behavior.

20. A smooth face parallel to the [001] stacking axis and forming a small dihedral angle with (010) was occasionally observed. This face is attributed to twinning, as its morphology and surface topography appear to be a mirror image of the aforementioned (010) plane.
21. The intermolecular bonding energy ϕ[uvw] is defined as the projection of the global solid state bonding interaction Φ along the [uvw] direction.
22. (a) P. Hartman and W.G. Perdok, *Acta Cryst.* **8**, 49 (1955). (b) P. Hartman and W.G. Perdok, *Acta Cryst.* **8**, 521 (1955). (c) P. Hartman and W.G. Perdok, *Acta Cryst.* **8**, 525 (1955).
23. (a) B.B. Mandelbrot, *The Fractal Geometry of Nature*, (Freeman, San Francisco, 1979). (b)*The Fractal Approach to Heterogeneous Chemistry*, D. Avnir, Ed. (John Wiley & Sons, Chichester, 1989).
24. The authors would like to acknowledge the support of the Office of Naval Research and the Center for Interfacial Engineering (NSF Engineering Research Centers Program). ACH would like to acknowledge the Upjohn Company for support in the form of an Upjohn Fellowship during 1992-93.

Figure Captions

Figure 1: AFM image of a (TTF)$Br_{0.76}$ crystal tip growing on HOPG with [001] parallel to the basal plane of graphite: (a) image of crystal tip with assigned planes; (b) surface plot of AFM height data illustrating the absolute crystal dimensions (crystal height corresponds to 7500 Å); (c) molecular resolution on the (010) face (raw data); (d) after fourier filtering. The molecular packing of (010) is superimposed on (d).

Figure 2: Nanoscopic surface morphology exhibited by exposed faces of (TTF)$Br_{0.76}$ during growth on HOPG: (a) surface structure and (b) molecular packing of the (010) face. The AFM image consists of [001] ledges formed from large, molecularly smooth (010) terraces intersected by steps with heights of 6.3 - 7.2 Å; (c) surface structure and (d) molecular packing of the $(\bar{3}10)$ face. The AFM image reflects a high ledge density on $(\bar{3}10)$ with ledges along [001] and kinks along $[\bar{1}\bar{3}0]$. The step heights of the ledges are 15 - 21 Å , corresponding to two or three TTF layers. The TTF cation stacks and Br^- anions are shown in (b) and (d), but the TTF hydrogen atoms have been omitted for clarity. The vertical striations on the extreme left of the AFM images are due to cantilever oscillation resulting from high feedback.

Figure 3: Images of triangular islands appearing on the (011) face of (TTF)$Br_{0.76}$ during growth: (a) AFM image of oriented triangular islands on (011), also indicating the $[13\bar{3}]$ zone axis that lies along the intersection of the (011) and $(\bar{3}10)$ planes; (b) aggregation of the triangular nuclei on (011); (c) the same region as in (b) after 60 seconds (several islands exhibit a Sierpinski Gasket self-similarity); (d) and (e) images of the triangular nuclei before and after their transformation to the rectangular raft morphology. The images in (a), (b) and (c), and (d) and (e), were obtained on different crystals in separate experiments. For reference, the angle between the $[13\bar{3}]$ direction and the edge of the triangles (experimentally measured value of 23 ± 5^{o}) is indicated in white on panels (a) and (b).

Figure 4: Molecular packing of the (011) face of (TTF)$Br_{0.76}$. The intersection of the (011) face with the $(\bar{3}10)$ and (210) faces is defined by the $[13\bar{3}]$ and $[\bar{1}2\bar{2}]$ zone axes, respectively. The

molecular kink sites on (011) are indicated by the open circles. The orientation and shape of the triangular nuclei depicted in Figure 3 are identical to the triangle constructed here from the kink sites defined by the solid lines (denoted as A). The angle subtended by the [13$\bar{3}$] zone axis and the upper edge of the triangle is 23°. The orientation that would result from the triangular array of kinks defined by the dashed lines (denoted as B) is not observed. Due to the monoclinic symmetry of (TTF)$Br_{0.76}$, orientations A and B are not crystallographically equivalent. The TTF hydrogen atoms and the Br^- anions have been omitted for clarity

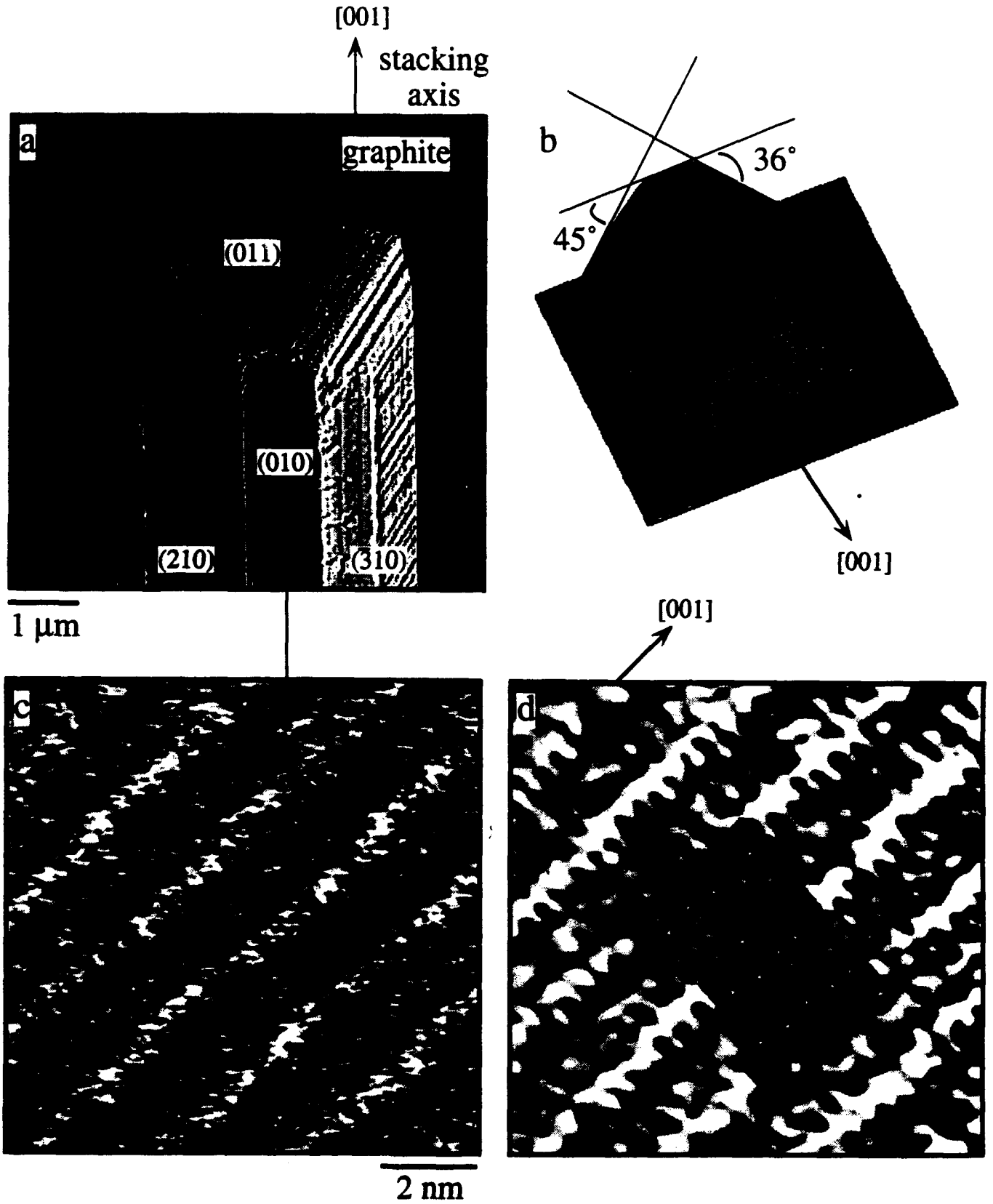
[001]
stacking axis
a
graphite
(011)
(010)
(210)
(310)
1 μm
b
36°
45°
[001]
[001]
c
d
2 nm

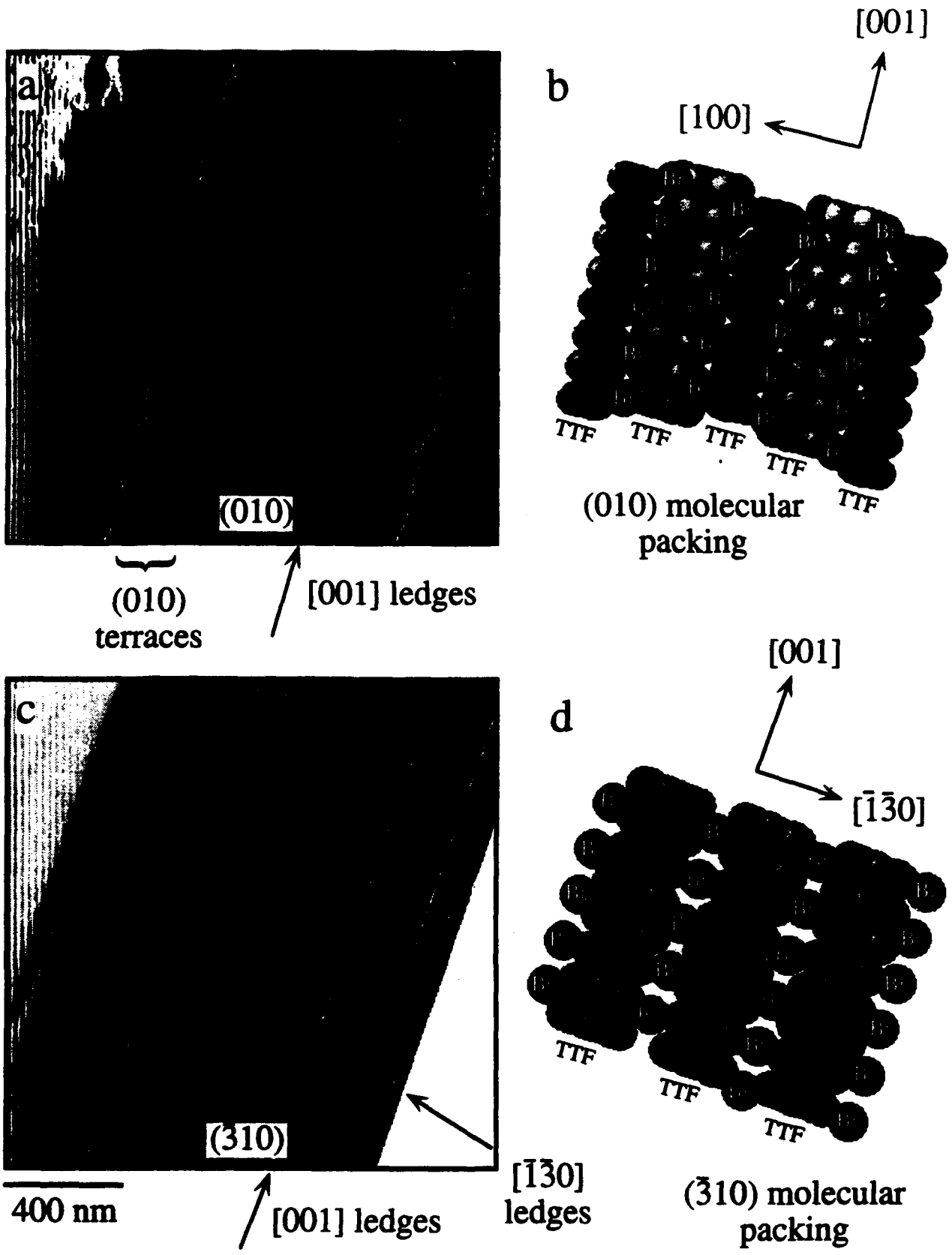
a
(010)
(010)
terraces
[001] ledges
b
[001]
[100]
TTF
TTF
TTF
TTF
TTF
(010) molecular
packing
c
(310)
400 nm
[001] ledges
[1̄30]
ledges
d
[001]
[1̄3̄0]
TTF
TTF
TTF
(3̄10) molecular
packing

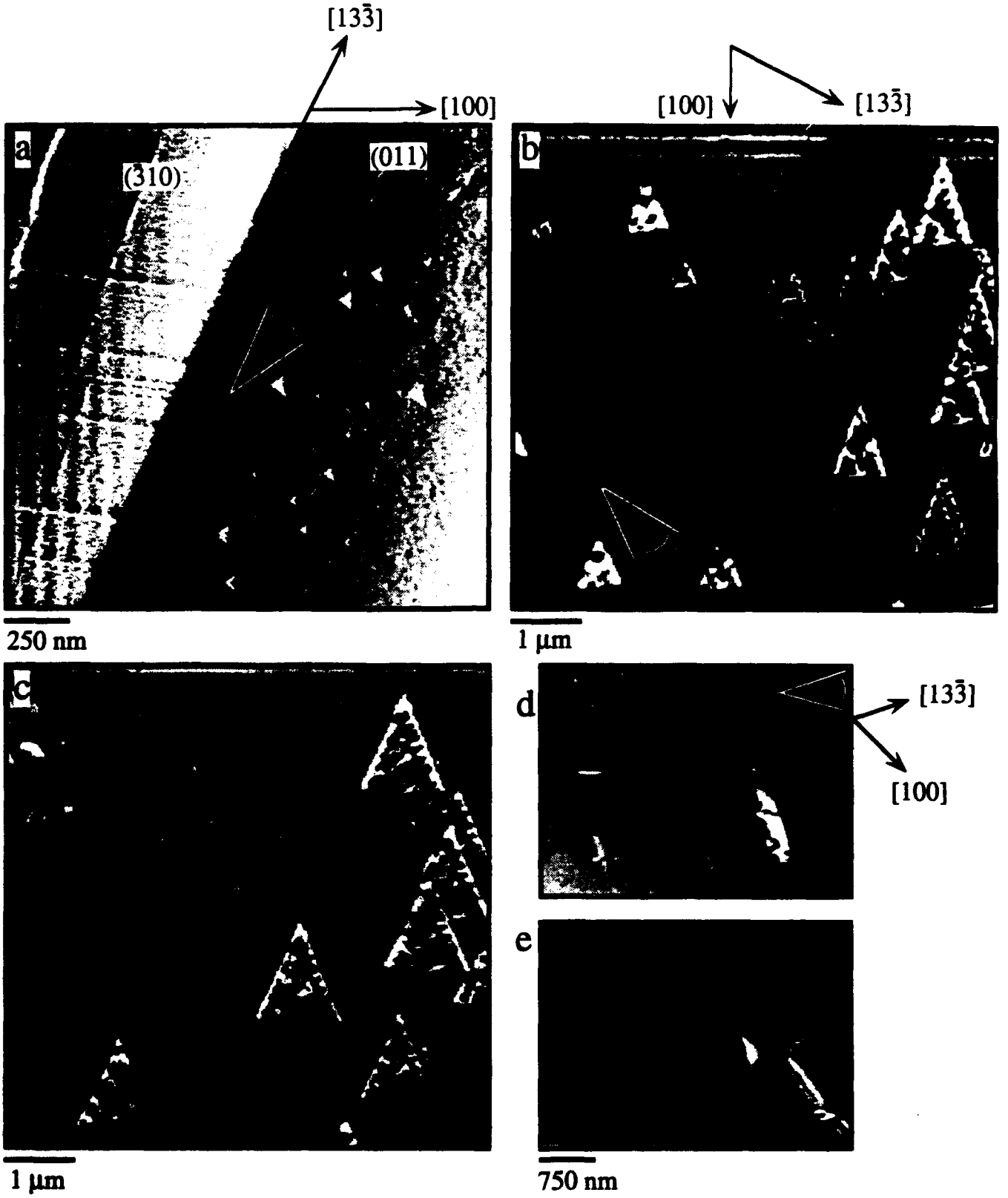
[13$\bar{3}$]
[100]
a
(310)
(011)
250 nm
[100]
[13$\bar{3}$]
b
1 µm
c
1 µm
d
[13$\bar{3}$]
[100]
e
750 nm

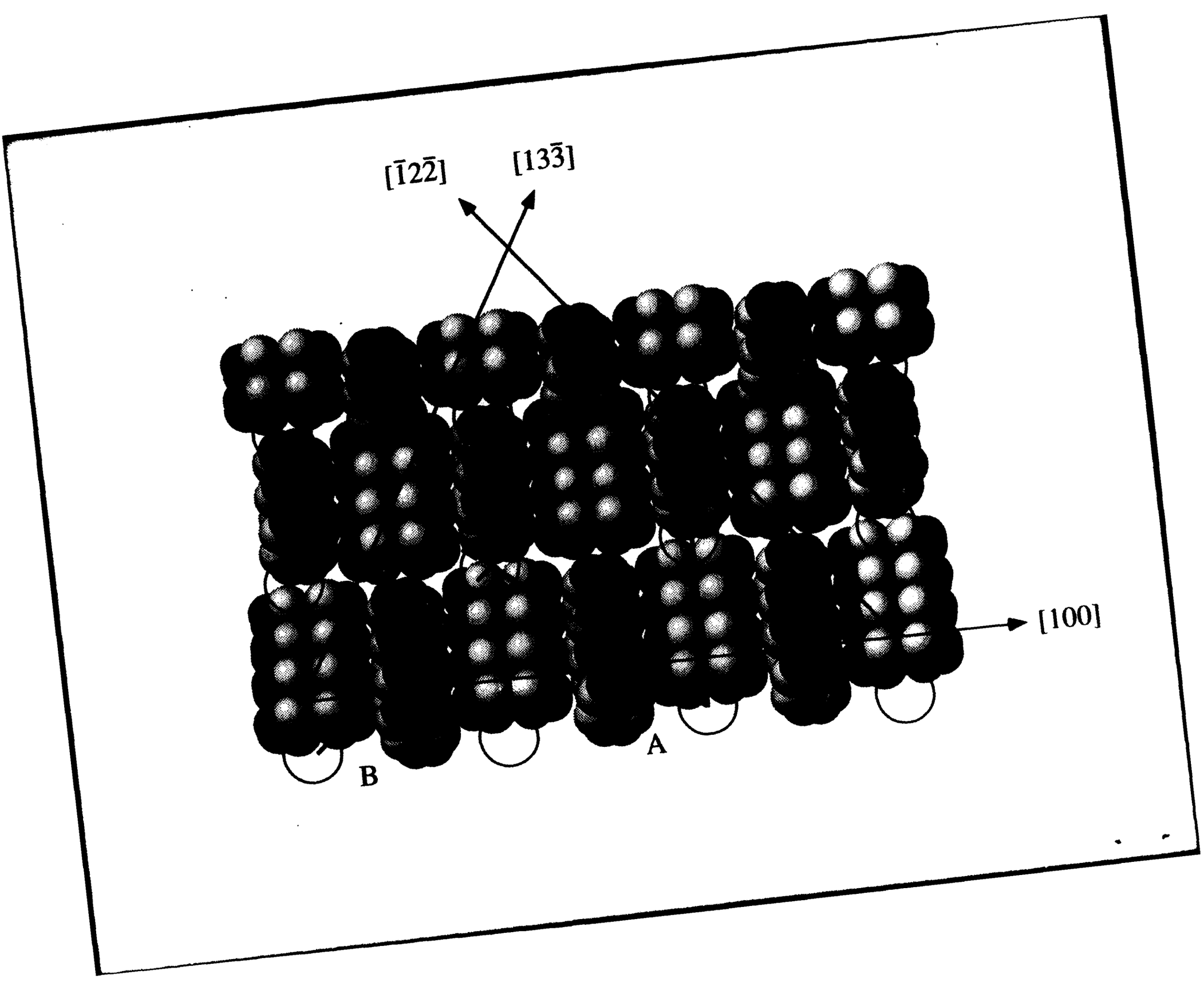
[$\bar{1}2\bar{2}$]
[$13\bar{3}$]
[100]
A
B